

## *ggh* variations

Adam Martin<sup>1</sup> and Michael Trott<sup>1,2</sup>

<sup>1</sup>*Department of Physics, University of Notre Dame, Notre Dame, Indiana 46556, USA*

<sup>2</sup>*Niels Bohr Institute, University of Copenhagen, Blegdamsvej 17, DK-2100 Copenhagen, Denmark*

(Received 2 November 2021; accepted 27 January 2022; published 8 April 2022)

We examine how subleading results in the operator and loop expansion for  $\sigma(\mathcal{G}\mathcal{G} \rightarrow h)$  in the Standard Model effective field theory (SMEFT) inform theoretical error estimates when studying this production channel in global SMEFT studies. We also discuss the relationship between geometric SMEFT results and the  $\kappa$  formalism.

DOI: [10.1103/PhysRevD.105.076004](https://doi.org/10.1103/PhysRevD.105.076004)

### I. INTRODUCTION

The Standard Model (SM) is an incomplete description of observed phenomena in nature. It must be extended to account for neutrino masses. This fact implies that new physics will couple to the SM. In addition, the hierarchy problem also argues for an extended sector of new physics at higher energy scales ( $\Lambda$ ), if the origin of neutrino masses is associated with such scales. As the exact origin of neutrino masses and the solution of the hierarchy problem are unknown, and certainly experimentally unverified, it is useful to think of the SM as an effective field theory (EFT) for data analysis with characteristic energies around the electroweak scale:  $\bar{v}_T \equiv \sqrt{2\langle H^\dagger H \rangle}$ .

The Standard Model effective field theory (SMEFT) is based on the low-energy assumptions that physics beyond the SM is present at scales  $\Lambda > \bar{v}_T$ , and that there are no light hidden states in the spectrum with couplings to the SM. A  $SU(2)_L$  scalar doublet ( $H$ ) with hypercharge  $y_h = 1/2$  is assumed to be present in the EFT. A power counting expansion in the ratio of scales  $q^2/\Lambda^2 < 1$ , follows with  $q^2$  a kinematic invariant associated with experimental measurements in the domain of validity of the EFT. These low-energy assumptions define a theory—the SMEFT—with the Lagrangian

$$\begin{aligned} \mathcal{L}_{\text{SMEFT}} &= \mathcal{L}_{\text{SM}} + \mathcal{L}^{(5)} + \mathcal{L}^{(6)} + \mathcal{L}^{(7)} + \dots, \\ \mathcal{L}^{(d)} &= \sum_i \frac{C_i^{(d)}}{\Lambda^{d-4}} \mathcal{Q}_i^{(d)} \quad \text{for } d > 4. \end{aligned} \quad (1)$$

---

*Published by the American Physical Society under the terms of the [Creative Commons Attribution 4.0 International](https://creativecommons.org/licenses/by/4.0/) license. Further distribution of this work must maintain attribution to the author(s) and the published article's title, journal citation, and DOI. Funded by SCOAP<sup>3</sup>.*

The operators  $\mathcal{Q}_i^{(d)}$  are labeled with a mass dimension  $d$  superscript and multiply unknown Wilson coefficients  $C_i^{(d)}$ , which predict patterns of corrections to the SM. The Wilson coefficients  $C_i^{(d)}$  take on specific values as a result of the  $q^2/\Lambda^2 < 1$  Taylor-expanded effects of physics beyond the SM. As the nature of physics beyond the SM is unknown, we treat the Wilson coefficients and the unknown  $\Lambda$  as free parameters to fit and constrain from the experimental data. This effectively treats the SMEFT as its own bottom-up-effective field theory. For compact dimensionless notation we define  $\tilde{C}_i^{(d)} \equiv C_i^{(d)} \bar{v}_T^{d-4} / \Lambda^{d-4}$ . The SM Lagrangian notation and conventions are consistent with Refs. [1–6]. The sum over  $i$ , after nonredundant operators are removed with field redefinitions of the SM fields, runs over the operators in a particular operator basis. We use the Warsaw basis [1,2] for  $\mathcal{L}^{(6)}$  in this paper.

When projecting constraints from global SMEFT fits onto the Wilson coefficients,<sup>1</sup> one might expect to always use a theoretical prediction of the highest order in the operator and the loop expansion. However, as one goes to higher order in the SMEFT expansions, the number of unknown parameters continually increases in a particular measurement, increasing the resulting fit spaces. This issue is not substantially ameliorated when combining multiple measurements, as each measurement has this challenge of theoretical interpretation. It is necessary to truncate the expressions to draw meaningful conclusions. The power counting of an EFT has a central role as it organizes the infinite number of parameters that enter the predictions into sets that are appropriate to retain when an approximate theoretical precision (chosen to be better than the current experimental precision) is used to interface with the data. For global SMEFT studies, the most straightforward choice

---

<sup>1</sup>For some recent studies of this form, see Refs. [7–13].

is to retain all linear  $\mathcal{L}^{(6)}$  interference terms with the SM amplitudes.

However, for  $\sigma(\mathcal{GG} \rightarrow h)$ , this choice faces challenges. Because the SM amplitude itself is loop level, parts of the SMEFT calculation that interfere with the SM—such as the piece linear in  $(\mathcal{L}^{(6)})$ —are suppressed compared to quadratic terms  $[(\mathcal{L}^{(6)})^2]$ . The quadratic term is accompanied by a factor of  $(\bar{v}_T/\Lambda)^2$  relative to the interference piece, but for low  $\Lambda$  this may not be enough to compensate for the loop factor difference. This interplay of loop factors and  $\bar{v}_T/\Lambda$  can be further exacerbated if one assumes hierarchical Wilson coefficients, due to “tree-loop” matching scenarios, as has been shown to arise in many UV matching scenarios [14–16] and, more generally, follows from the conditions of naive ( $d \leq 4$ ) renormalizability being imposed on all UV physics at higher scales [17]. Specifically, if the relevant dimension-six coefficients are small as the result of UV matching, while the dimension-eight coefficients are order one, both the  $\mathcal{L}^{(6)}$  and  $(\mathcal{L}^{(6)})^2$  contributions to  $\sigma(\mathcal{GG} \rightarrow h)$  may be subdominant to  $(\mathcal{L}^{(8)})$  terms. This argument applies to all SM loop processes; however, we will focus on  $\sigma(\mathcal{GG} \rightarrow h)$  given the prominent role it plays in SMEFT global fits. An analysis of  $\Gamma(h \rightarrow \gamma\gamma)$  is given in Appendix B.

In this paper, we explore how choices about where the SMEFT calculation is truncated when interpreting experimental results and what is assumed about the hierarchy among Wilson coefficients affect the theoretical error on  $\sigma(\mathcal{GG} \rightarrow h)$ . There is no unique answer to defining an error estimate for neglected higher-order terms in a perturbative expansion, and a reasonable error estimate is never an assertion of precise and exact knowledge of all higher-order terms.<sup>2</sup> Here we restrict ourselves to a well-defined procedure for defining such an error, maximally informed by the actual higher-order results, when such results are available in the literature. For  $\sigma(\mathcal{GG} \rightarrow h)$ , the result including both  $\mathcal{L}^{(6)}$  effects to one-loop order [ $\mathcal{O}(1/16\pi^2\Lambda^2)$ ] and the complete set of  $\mathcal{L}^{(8)}$  effects [ $\mathcal{O}(1/\Lambda^4)$ ] was recently developed in Ref. [18].

## II. $\sigma(\mathcal{GG} \rightarrow h)$ TO $\mathcal{O}(1/\Lambda^4)$ , $\mathcal{O}(1/16\pi^2\Lambda^2)$

It is appropriate to organize  $\mathcal{L}_{\text{SMEFT}}$  as specific composite operator kinematics, with scalar dressings that do not introduce new kinematics, to identify the full set of  $\mathcal{O}(1/\Lambda^4)$  corrections. This is the geoSMEFT approach developed in Refs. [6,19–21] where scalar-field-dependent field-space connections  $G_i$  multiply composite operator forms  $f_i$  as

$$\mathcal{L}_{\text{SMEFT}} = \sum_i G_i(I, A, \phi \dots) f_i. \quad (2)$$

<sup>2</sup>Such theoretical error estimates are still meaningful. Including such theoretical errors, when they can be estimated, is a standard practice in EFT studies for decades.

Powers of  $D^\mu H$  are included in  $f_i$ ,  $I$  and  $A$  represent possible  $SU(2)_L$  and  $SU(3)$  group structures, and  $\phi_{1,2,3,4}$  are components of the Higgs  $H$  field. The kinematic dependence is factorized into the  $f_i$  and the rescalings by  $G_i$ . The geoSMEFT is defined to all orders in the  $\sqrt{2\langle H^\dagger H \rangle}/\Lambda$  expansion for low  $n$ -point functions ( $n \leq 3$ ), which is sufficient for the case of interest here.<sup>3</sup> In addition, as the loop expansion and the operator expansion are not independent at subleading order in the SMEFT [18], it is necessary to formulate  $\mathcal{O}(1/16\pi^2\Lambda^2)$  corrections in the SMEFT in a manner consistent with the geoSMEFT organization higher-order  $\mathcal{O}(1/\Lambda^4)$  physics. This is best accomplished in the background field method approach to gauge fixing in the SMEFT [19,22–24].

The general Higgs-gluon field space metric is defined as [6]

$$\mathcal{L}_{\text{SMEFT}} \supset -\frac{1}{4} \kappa(\phi) G^{\mathcal{A},\mu\nu} G_{\mathcal{A},\mu\nu}, \quad (3)$$

with  $\mathcal{A}$  running over  $\{1\dots 8\}$  and

$$\kappa(\phi) = \left( 1 - 4 \sum_{n=0}^{\infty} C_{\text{HG}}^{(6+2n)} \left( \frac{\phi^2}{2} \right)^{n+1} \right). \quad (4)$$

For the gluon field strength and coupling, the transformations to canonically normalized fields at all  $1/\Lambda^n$  orders are given by

$$G^{A,\nu} = \sqrt{\kappa} \mathcal{G}^{\mathcal{A},\nu}, \quad (5)$$

$$\bar{g}_3 = g_3 \sqrt{\kappa}. \quad (6)$$

We return to the nature of these field redefinitions below.

We write the amplitude perturbation to the process as [18]

$$\begin{aligned} \mathcal{A}_{\mathcal{GG}h} &= \mathcal{A}_{\text{SM}}^{\mathcal{GG}h} + \langle \mathcal{GG} | h \rangle_{\mathcal{O}(\bar{v}_T^2/\Lambda^2)}^0 + \langle \mathcal{GG} | h \rangle_{\mathcal{O}(\bar{v}_T^2/\Lambda^2)}^1 \\ &+ \langle \mathcal{GG} | h \rangle_{\mathcal{O}(\bar{v}_T^4/\Lambda^4)}^0 + \dots, \end{aligned} \quad (7)$$

where each of the expressions for  $\mathcal{A}_{\text{SM}}^{\mathcal{GG}h}$ ,  $\langle \mathcal{GG} | h \rangle_{\mathcal{O}(\bar{v}_T^2/\Lambda^2)}^0$ ,  $\langle \mathcal{GG} | h \rangle_{\mathcal{O}(\bar{v}_T^2/\Lambda^2)}^1$ , and  $\langle \mathcal{GG} | h \rangle_{\mathcal{O}(\bar{v}_T^4/\Lambda^4)}^0$  are now known in a consistent set of perturbations in the loop (indicated with a superscript number) and operator expansion (indicated with a subscript). The SM result itself  $\mathcal{A}_{\text{SM}}^{\mathcal{GG}h}$  also has a perturbative expansion, and is often determined in an operator expansion with a heavy top limit taken. Here we use the SM result as reported in Ref. [18], which is not the highest-order SM result

<sup>3</sup>The geoSMEFT formulation currently offers the only theoretical framework to calculate consistently to  $\mathcal{O}(1/\Lambda^4)$ . As the loop and operator expansion are not independent (see Ref. [18]), this means that these results are consistently formulated to orders  $\mathcal{O}(1/16\pi^2\Lambda^2)$  and  $\mathcal{O}(1/\Lambda^4)$  in the geoSMEFT, marking it as a unique theoretical framework enabling such results (at this time).

known, but it is sufficient for our error estimate purposes. The important structure of the series expansions is the appearance of new parameters perturbing the SM in the series expansion, and the appearance of perturbative loop correction factors  $\propto 1/16\pi^2$  and the operator expansion corrections  $\propto \bar{v}_T^2/\Lambda^2$  at higher orders in the double series expansion.

The operator expansion of the field space connection introduces sensitivity to one new  $\mathcal{L}^{(8)}$  operator at subleading order:  $\mathcal{Q}_{\text{HG}}^{(8)}$ . In addition, several cross terms of the form  $\mathcal{L}^{(6)} \times \mathcal{L}^{(6)}$ , including an important contribution from  $(C_{\text{HG}}^{(6)})^2$ , are present in the expansion of  $\sqrt{\kappa}$ . Similarly, the SMEFT loop expansion introduces corrections to the Wilson coefficient already present at leading order ( $C_{\text{HG}}^{(6)}$ ) and also introduces the new parameters ( $C_{H\Box}^{(6)}$ ,  $C_{HD}^{(6)}$ ,  $C_{Hu}^{(6)}$ ,  $C_{uG}^{(6)}$ ), whose operator definitions are

$$\begin{aligned} \mathcal{Q}_{H\Box}^{(6)} &= (H^\dagger H)\Box(H^\dagger H), \\ \mathcal{Q}_{HD}^{(6)} &= (H^\dagger D_\mu H)^*(H^\dagger D_\mu H), \\ \mathcal{Q}_{Hu}^{(6)} &= (H^\dagger i\overleftrightarrow{D}_\mu H)(\bar{u}_r\gamma^\mu u_r), \\ \mathcal{Q}_{uG}^{(6)} &= (\bar{q}_3\sigma^{\mu\nu}T^A u_3)\tilde{H}G_{\mu\nu}^A, \end{aligned} \quad (8)$$

where  $r, s$  run over 1,2,3 for the up ( $u$ ), charm ( $c$ ), and top ( $t$ ) quark flavor labels, and  $\tilde{H}_j = \epsilon_{jk}H^{\dagger,k}$ . For the remaining notational conventions, consult Refs. [1–6]. Dependence on

$$\delta G_F^{(6)} = \frac{1}{\sqrt{2}} \left( \tilde{C}_{ee}^{(3)} + \tilde{C}_{\mu\mu}^{(3)} - \frac{1}{2} (\tilde{C}'_{\mu e e \mu} + \tilde{C}'_{e \mu \mu e}) \right) \quad (9)$$

is also present due to a redefinition of the input parameter vacuum expectation value, introducing a further dependence on the coefficients of

$$\begin{aligned} \mathcal{Q}_{pr}^{(3)} &= (H^\dagger i\overleftrightarrow{D}_\mu H)(\bar{l}_p\tau^I\gamma^\mu l_r), \\ \mathcal{Q}'_{pprp} &= (\bar{l}_p\gamma^\mu l_r)(\bar{l}_r\gamma^\mu l_p). \end{aligned} \quad (10)$$

The explicit expression defined/developed in Ref. [18] is

$$\begin{aligned} \frac{\sigma_{\text{SMEFT}}^{\hat{\alpha}}(\mathcal{G}\mathcal{G} \rightarrow h)}{\sigma_{\text{SM}}^{\hat{\alpha},1/m^2}(\mathcal{G}\mathcal{G} \rightarrow h)} &\simeq 1 + 519\tilde{C}_{\text{HG}}^{(6)} + 504\tilde{C}_{\text{HG}}^{(6)} \left( \tilde{C}_{H\Box}^{(6)} - \frac{1}{4}\tilde{C}_{HD}^{(6)} \right) + 8.15 \times 10^4 (\tilde{C}_{\text{HG}}^{(6)})^2 + 504\tilde{C}_{\text{HG}}^{(8)} \\ &+ 1.58 \left( \tilde{C}_{H\Box}^{(6)} - \frac{1}{4}\tilde{C}_{HD}^{(6)} \right) + 362\tilde{C}_{\text{HG}}^{(6)} - 1.59\tilde{C}_{uH}^{(6)} - 12.6\text{Re}\tilde{C}_{uG}^{(6)} - 1.12\delta G_F^{(6)} - 7.70\text{Re}\tilde{C}_{uG}^{(6)} \log\left(\frac{\hat{m}_h^2}{\Lambda^2}\right) \\ &- 0.19\text{Re}\tilde{C}_{dG}^{(6)} \log\left(\frac{\hat{m}_h^2}{\Lambda^2}\right) - 0.09\text{Re}\tilde{C}_{dG}^{(6)} + 3.54\tilde{C}_{dH}^{(6)}. \end{aligned} \quad (11)$$

The expression is reported in the  $\hat{\alpha}_{ew}$  input parameter scheme, but input parameter scheme dependence is negligible in this expression. In this expression, we have omitted contributions from Yukawa couplings other than  $y_t$  as they are numerically negligible.<sup>4</sup> The leading dependence on  $\tilde{C}_{\text{HG}}^{(6)}$  has a numerical coefficient of 519; this coefficient is a few percent different than the coefficient of  $\tilde{C}_{\text{HG}}^{(8)}$  as in  $\mathcal{A}_{\text{SM}}^{\mathcal{G}\mathcal{G}h}$  we have expanded in the heavy top limit and retained a higher-order term in the former.

To explore the effect of retaining higher-order terms in the interpretation of a projected measurement of  $\sigma(\mathcal{G}\mathcal{G} \rightarrow h)$  from the production and decay of the Higgs with theory errors, we consider three cases. In each case, the full expression in Eq. (11) is broken up into a piece used to project experimental constraints, and the remainder, which represents neglected higher-order terms. The three cases are as follows:

- (i) Interpret experimental data using the linear  $\mathcal{L}^{(6)}$  interference term only, which in this case is just the  $C_{\text{HG}}^{(6)}$  contribution. We include both the tree-level and one-loop corrections  $\propto C_{\text{HG}}^{(6)}$ .
- (ii) Interpret experimental data keeping the  $C_{\text{HG}}^{(6)}$  interference term plus the  $(C_{\text{HG}}^{(6)})^2$  “squared” piece.
- (iii) In addition to the pieces in ii), retain the  $C_{\text{HG}}^{(8)}$  contribution.

While case (i) is the standard, the validity and features of cases (ii) and (iii) warrants more study before jumping into numerics.

### III. QUADRATIC FITS IN LOOP PROCESSES AND TREE-LEVEL PROCESSES IN THE SM

Retaining terms in the SMEFT prediction for the practical purpose of making the theoretical precision greater than the experimental precision in an observable would naively argue for retaining the  $(C_{\text{HG}}^{(6)})^2$  term in

<sup>4</sup>We also ignore all  $CP$ -odd operators due to strong, low-energy constraints; see Refs. [25,26].

Eq. (11) unless  $C_{HG}^{(6)} \ll 1$ , due to (for example) a loop suppression in matching.

On the other hand, retaining only a subset of terms at an order in a power-counting expansion is formally ill defined in EFT, as a field redefinition on a SM field  $F$

$$F \rightarrow F'[1 + \mathcal{O}(1/\Lambda^n)] \quad (12)$$

can change the set of parameters retained (or remove the parameters entirely), resulting in ambiguous predictions. This point was recently stressed in Ref. [27].

For example, a field redefinition involving  $C_{HG}^{(6)}$  is allowed (and even required on the gluon field to take the theory to the canonical form) in Eq. (5) at  $\mathcal{O}(1/\Lambda^4)$ . This field redefinition on  $A_{SM}^{ggh}$  cancels order by order against the simultaneous redefinition of the gauge coupling at all orders [see Eq. (5)]. Applied to  $Q_{HG}$ , the redefinition

$$G_{\mu\nu}^A \rightarrow G_{\mu\nu}^A(1 + \mathcal{O}(C_{HG}^{(6)}v_T^4/\Lambda^4)) \quad (13)$$

does not cancel and generates  $\mathcal{O}((C_{HG}^{(6)})^2/\Lambda^4)$  effects that are ambiguous until the theory is fully defined at  $\mathcal{O}(1/\Lambda^4)$ . However, when determining the cross section, the ambiguous  $\mathcal{O}((C_{HG}^{(6)})^2/\Lambda^4)$  terms enter via interference with the (loop-suppressed) SM amplitude  $A_{SM}^{ggh}$  and are therefore numerically suppressed (regardless of how one chooses the Wilson coefficients) compared to the quadratic (self-square) contribution,  $(Q_{HG})^2$ . In this sense, quadratic fits to *loop-suppressed processes in the SM*, although formally inconsistent in the treatment of the power counting, are only sensitive to a small numerical error in some cases. This is the case when considering the Higgs-gluon field space connection, and constraints on  $Q_{HG}^{(6)}$  retaining quadratic terms are of increased interest as a result.

This reasoning only applies to  $Q_{HG}^{(6)}$ ,  $(Q_{HG}^{(6)})^2$  when studying constraints on  $\sigma(\mathcal{GG} \rightarrow h)$  and fails—in the sense that relative numerical errors are subsequently  $\mathcal{O}(1)$ —for all other Wilson coefficient dependence in Eq. (11). In particular, it fails for dependence on the Wilson coefficient of  $Q_{HG}^{(8)}$ .

#### IV. $\kappa$ RESCALINGS AND geoSMEFT

It is interesting to consider the possibility of projecting experimental constraints onto the entire Higgs-Gluon field space connection  $\kappa$  [defined in Eq. (3)], and the relation of such a procedure to the so called “ $\kappa$  formalism” developed in Refs. [28–32].<sup>5</sup>

In the “ $\kappa$  formalism,” the coefficient of the three point  $g$ - $g$ - $h$  coupling is treated as a parameter that experiments fit to. We can map the geoSMEFT expression (3) into this form by expanding to linear order in  $\phi$ ,

<sup>5</sup>The coincidence in common  $\kappa$  notion should not be over interpreted.

$$\kappa_{\text{geoSMEFT}} = \left\langle \frac{\delta\kappa}{\delta h} \right\rangle \langle \kappa \rangle = -4 \frac{\tilde{C}_{HG}^{(6)}}{\bar{v}_T} - 4 \frac{\tilde{C}_{HG}^{(8)}}{\bar{v}_T} + 8 \frac{(\tilde{C}_{HG}^{(6)})^2}{\bar{v}_T}. \quad (14)$$

One may expect that  $\kappa_{\text{geoSMEFT}}$  is less sensitive to Wilson coefficient hierarchies, such as the tree/loop scenario, where  $C_{HG}^{(8)} \sim 16\pi^2 C_{HG}^{(6)}/g^2$ , since all effects are lumped into a single coefficient. However, when inspecting the cross section ratio [Eq. (11)],  $\kappa_{\text{geoSMEFT}}$  is not manifest. Treating the  $g$ - $g$ - $h$  vertex as a single object misses subtleties (such as which terms interfere with the SM and which do not) that the operator expansion catches.

Extracting the components of Eq. (11) that have the largest numerical factors and fewest powers of the  $\tilde{C}_i$ , we find some middle ground: a quantity that involves only a few Wilson coefficients, yet is derived at the cross section level and so captures information about interference with the SM,

$$\frac{\sigma_{\text{SMEFT}}^{\hat{\alpha}}(\mathcal{GG} \rightarrow h)}{\sigma_{\text{SM}}^{\hat{\alpha},1/m_t^2}(\mathcal{GG} \rightarrow h)} \simeq 1 + 881\Sigma_k + \dots$$

$$\Sigma_k = [\tilde{C}_{HG}^{(6)} + 0.57\tilde{C}_{HG}^{(8)} + 93(\tilde{C}_{HG}^{(6)})^2]. \quad (15)$$

The coefficient 881 is the sum of the tree0level  $\tilde{C}_{HG}^{(6)}$  term plus the retained loop correction for this operator; the relative 0.57 in front of  $\tilde{C}_{HG}^{(8)}$  comes about because terms of  $\mathcal{O}(\bar{v}_T^4/16\pi^2\Lambda^4)$  were not included in Ref. [18]. Had these terms been included, the factor  $0.57 \rightarrow \sim 1$ .

The combination  $\Sigma_k$  is present for other phenomena involving a single Higgs. For example, the significant numerical dependence on  $\tilde{C}_{HG}^{(6)}$  in the Higgs width in the SMEFT [33] can be rescaled out using the results in [18] as

$$\frac{\Gamma_{h,\text{full}}^{\text{SMEFT}}}{\Gamma_h^{\text{SM}}} \simeq 1 + 50.6\tilde{C}_{HG}^{(6)} + \dots$$

$$\simeq 1 + 88\Sigma_k - 6.7\tilde{C}_{HG}^{(6)} + \dots \quad (16)$$

The total Higgs width has a very significant dependence on  $(\tilde{C}_{HG}^{(6)})^2$  in the SMEFT via  $\Sigma_k$ . The subtraction of an explicit dependence on  $\tilde{C}_{HG}^{(6)}$  is due to the difference in the one-loop correction in  $\sigma(\mathcal{GG} \rightarrow h)$  vs  $\Gamma(h \rightarrow \mathcal{GG})$  at one loop, as specified in Ref. [18].

To break the parameter degeneracy built into  $\Sigma_k$  experimentally one needs to consider a process with more than one Higgs field exchange at tree level in a Feynman diagram, or further loop corrections breaking degeneracies. For example, the parameter degeneracy of  $\tilde{C}_{HG}^{(6)}$  in  $\sigma(\mathcal{GG} \rightarrow h)$  and  $\Gamma(h \rightarrow \mathcal{GG})$  is already weakly broken by a one-loop correction, as shown in Eq. (16).

In general, the geoSMEFT approach is closely related to the  $\kappa$  formalism where rescalings of SM processes occur with common kinematic dependence in the SM and an

effective field theory extension. It has been argued that the specific implementation of this idea in Ref. [32] is directly mappable to the HEFT (Higgs Effective Field Theory) formalism in Refs. [34,35]. The geoSMEFT also provides a rescaling generalization of the SM which allows a field theory interpretation of the  $\kappa$  formalism in Ref. [32], and that can also be extended to non-SM kinematics in a well-defined way. The resummation of higher orders in  $\bar{v}_T^2/\Lambda^2$  in the geometric dressings of the composite operator forms also breaks the relationships between SMEFT corrections enforced by linearly realized  $SU(2)_L$  symmetry, as in the HEFT. However, in the geoSMEFT case the expansion back to a linear-realization SMEFT is direct and follows from Taylor expanding the geoSMEFT field space connections.

## V. NUMERICAL STUDY

To more quantitatively understand the impact of including higher-order terms in the interpretation of experimental  $\sigma(\mathcal{GG} \rightarrow h)$  data, we turn to numerics. Specifically, we study how the uncertainty—encapsulated by the remainder terms for the cases identified earlier—varies among the cases and as we change assumptions about the sizes of Wilson coefficients. We consider two different Wilson coefficient schemes: a) all Wilson coefficients set to the same value, and b) an ordering of the Wilson coefficients according to a tree-loop matching scheme. Defining the uncertainty in this fashion is consistent with the arguments in Refs. [18,20,36] and, in particular, Ref. [27].

Our first step is to focus our study on coefficients and  $\Lambda$  scales that are not already experimentally excluded. We do this by equating the retained piece of the SMEFT calculation in each case to the current experimental uncertainty on  $\mu_{ggh}$ , e.g., for case (i) we solve  $881\tilde{C}_{\text{HG}}^{(6)} = \delta\mu_{ggh}$ . To extract a rough minimum  $\Lambda_{\text{min}}$  scale from this, we plug in a value for  $C_{\text{HG}}^{(6)}$  according to a chosen Wilson coefficient sampling scheme. We take the Wilson coefficient constraint from a fit to  $\mu_{ggh}$ , using the constraint  $\mu_{ggh} = 1.04 \pm 0.09$  [37,38]. We use 0.09 as a rough error band to define relevant perturbations that are not experimentally disfavored when considering error estimates.<sup>6</sup>

<sup>6</sup>Note that significant cancellations can occur between terms in Eq. (11), lowering a naive compatibility scale, and this translates into cases where the theory error on the experimental projection of results onto  $C_{\text{HG}}^{(6)}$ , etc. is significantly higher. This is also qualitatively indicated with the blowing up of the theory error curve in Fig. 1. Such cancellations, leading to flat directions, are broken by considering top measurements [39] and in a global study are expected to be less relevant than the generic case considered here with a naive compatibility scale and no significant cancellations. Such potential cancellations, with a corresponding large theory error when canceling terms are neglected, are also illustrated by the variations in Figs. 2–4.

Next, we numerically evaluate the uncertainty for the three cases as a function of  $\Lambda > \Lambda_{\text{min}}$ . To avoid accidental cancellations, we assign values to the Wilson coefficients at each step by drawing them from Gaussian distributions centered at zero and with widths set by the Wilson coefficient scheme. Repeating this 10 000 times at each  $\Lambda$  step, we take the  $1\sigma$  width of the resulting Gaussian distribution as the theory error. This theory error is driven primarily by  $\Lambda$  and is, by design, restricted to scales that are still viable for a given coefficient choice. Switching to a flat distribution for sampling the Wilson coefficients leads to identical results. This is to be expected: evaluating the uncertainty in this way amounts to sampling the linear sum of multiple parameters, so the central limit theory dictates that the resulting error distribution will be Gaussian regardless of how the individual terms are sampled.

The resulting theory error is shown in Fig. 1. For the tree/loop Wilson coefficient matching scheme we use values of 1.0/0.01. For the matching scheme with all coefficients taken equal, we try two cases, all coefficients 0.01 and all 1.0. The  $\Lambda_{\text{min}}$  values for the cases are different,<sup>7</sup> but plotting the curves vs  $\Lambda/\Lambda_{\text{min}}$  hides shifts in  $\Lambda_{\text{min}}$  and allows all curves to be shown in one plot. The solid (all coefficients 0.01) and dotted (all coefficients 1.0) lines are nearly identical, as overall changes in the coefficients can be compensated—up to the terms containing  $\log(\Lambda^2)$ —by rescaling  $\Lambda_{\text{min}}$ .

When all coefficients are chosen equal, the error estimates in all of the cases are nearly identical. When coefficients are chosen with the tree/loop hierarchy, the error in case (iii) is roughly 2 times smaller than that in cases (i) and (ii). This difference is due to  $C_{\text{HG}}^{(8)}$ , a tree-level term as classified by Ref. [16], that is part of the uncertainty in cases (i) and (ii) but not in case (iii). The size and stability of the uncertainty curve for case (iii) under the two Wilson coefficient matching schemes makes the case for projecting experimental fit results onto  $\Sigma_\kappa$ . An alternative theory error analysis, fixing  $C_{\text{HG}}^{(6)}$  and sampling the higher-order terms using the method of Ref. [20], is shown in Appendix A.

As  $\Sigma_\kappa$  is not the complete  $\mathcal{O}(1/\Lambda^4)$  result, the obvious worry is that artifacts or ambiguities may be present. The analysis of Sec. III shows that field redefinition ambiguities can be present, but they are small. A second concern is that the combination of parameters retained introduces intrinsic basis choice dependence. For example, it has been shown in Refs. [20,36] that dependence on  $\lambda\bar{v}_T^2$  purely due to operator basis choice in matching a UV model onto the SMEFT cancels in observables, but could persist in inconsistent calculations to  $\mathcal{O}(1/\Lambda^4)$ . To check whether

<sup>7</sup>Explicitly, for all coefficients equal to 0.01,  $\Lambda_{\text{min}} = 2.43, 2.44, 2.45$  TeV for cases i), ii), and iii), respectively, while for all coefficients equal to 1.0,  $\Lambda_{\text{min}} = 24.3, 24.5, 24.5$  TeV and  $\Lambda_{\text{min}} = 2.43, 2.44, 2.90$  TeV for the tree/loop (1.0/0.01) scheme.

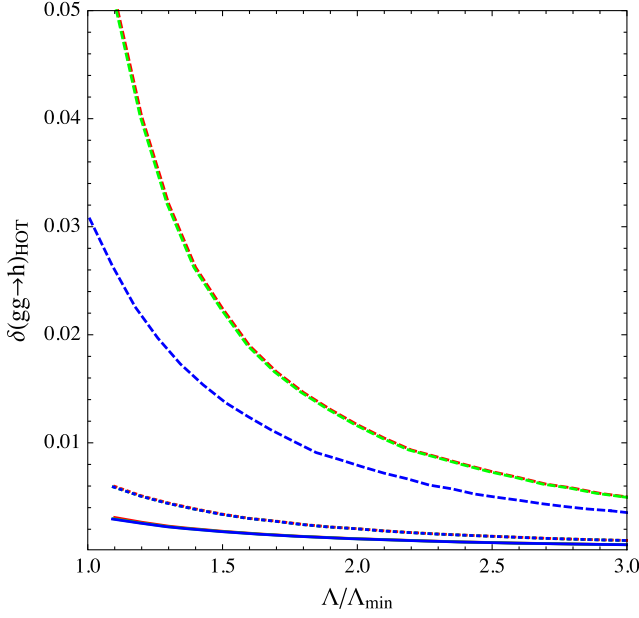


FIG. 1. Uncertainty on  $\sigma(gg \rightarrow h)$  from higher-order terms as a function of the new physics scale  $\Lambda$  relative to the minimum scale compatible with current experimental  $gg \rightarrow h$  data. We have broken the full  $\sigma(gg \rightarrow h)_{\text{SMEFT}}$  calculation of Ref. [18] into a calculation piece used to determine the compatibility scale and a higher-order-terms piece in three different ways. (i) First, we retain only the  $\mathcal{O}(1/\Lambda^2)$  interference term. (ii) Second, we include the interference term and pieces proportional to  $(C_{\text{HG}}^{(6)})^2$  in the retained result in the calculation to determine the compatibility scale. (iii) This is the same as in (ii), but the  $C_{\text{HG}}^{(8)}$  term is also included, which corresponds to  $\Sigma_\kappa$ . For a given set of retained terms, we determine the minimum scale by equating it with the current experimental uncertainty on  $\sigma(\mathcal{GG} \rightarrow h)$ . The curves shown are then generated by incrementing  $\Lambda$  above  $\Lambda_{\text{min}}$  and numerically evaluating the numerical error by plugging in coefficients according to a scheme and evaluating the neglected terms. The dashed lines correspond to the tree/loop scheme with values 1.0/0.01, the solid lines correspond to picking all coefficients equal to 0.01, and the dotted lines correspond to picking all coefficients equal to 1.0. Case (i) is shown in red, case (ii) in green, and case (iii) in blue. For the tree/loop scheme, the retained partitions (i) and (ii) are nearly identical, while all three cases are nearly identical when all coefficients are chosen equal (same color scheme for the cases).

or not this combination of terms introduces such an intrinsic basis dependence, we study a matching example.

## VI. MATCHING EXAMPLE

Consider integrating out  $\sigma$ , which couples to the SM as

$$\mathcal{L}_\sigma = \frac{1}{2}(\partial_\mu \sigma)^2 - \frac{1}{2}m_\sigma^2 \sigma^2 + \frac{ag_3^2 \sigma G_{\mu\nu}^A G^{A,\mu\nu}}{\Omega} + \Omega b H^\dagger H \sigma. \quad (17)$$

This is an example of a nonminimally coupled model, as discussed in Ref. [17]. Rewriting the Lagrangian as

$$\mathcal{L} = \mathcal{L}_{\text{SM}} - \frac{1}{2}\sigma(\partial^2 + m_\sigma^2)\sigma + \sigma B, \quad (18)$$

$$B = \frac{ag_3^2 G_{\mu\nu}^A G^{A,\mu\nu}}{\Omega} + \Omega d H^\dagger H \quad (19)$$

and using the results from Refs. [36,40] yields

$$\mathcal{L} = \mathcal{L}_{\text{SM}} + \frac{1}{2m_\sigma^2} B^2 + \frac{1}{2m_\sigma^4} B \partial^2 B + \mathcal{O}(m_\sigma^{-6}). \quad (20)$$

It is necessary for the condition  $b \ll \Omega/m_\sigma$  to be imposed for the expansion in  $1/m_\sigma$  to be convergent. The low-energy effects of this matching is to redefine the SM  $\lambda$ ,  $\bar{v}_T$ , and  $m_h$  as

$$\bar{v}_T^2 \rightarrow (v')^2 + \frac{b^2 \Omega^2 \bar{v}_T^2}{2\lambda m_\sigma^2}, \quad (21)$$

$$\lambda \rightarrow \lambda' - \frac{b^2 \Omega^2}{2m_\sigma^2}, \quad (22)$$

$$m_h^2 = 2\lambda \bar{v}_T^2 \quad (23)$$

$$\rightarrow 2\lambda'(v')^2 \left[ 1 - \frac{b^4 \Omega^4}{4(\lambda')^2 m_\sigma^4} \right]. \quad (24)$$

The remaining contributions come from expanding out  $B \partial^2 B$ . The effects include a contribution to the gluon self-interactions,

$$\frac{1}{2m_\sigma^4} \frac{a^2 g_s^4}{\Omega^2} [G_{\mu\nu}^A G^{A,\mu\nu}] \partial^2 [G_{\mu\nu}^A G^{A,\mu\nu}], \quad (25)$$

and the contribution to  $C_{H\Box}$  is

$$\frac{\Omega^2}{2m_\sigma^4} b^2 Q_{H\Box}. \quad (26)$$

A more interesting interaction comes from the cross term,

$$\frac{abg_s^2}{2m_\sigma^4} [G_{\mu\nu}^A G^{A,\mu\nu} \partial^2 (H^\dagger H) + \partial^2 (G_{\mu\nu}^A G^{A,\mu\nu}) (H^\dagger H)].$$

One can integrate by parts to arrange this contribution into the form

$$\frac{abg_s^2}{2m_\sigma^4} [2G_{\mu\nu}^A G^{A,\mu\nu} \partial^2 (H^\dagger H)]. \quad (27)$$

Expanding out,

$$\partial^2 (H^\dagger H) \rightarrow 2(D^\mu H^\dagger)(D_\mu H) + (D^2 H^\dagger)H + H^\dagger(D^2 H).$$

The first term does not contribute to  $\sigma(gg \rightarrow h)$ , while the remaining terms are equation-of-motion reducible to the combination of terms

$$2(\lambda \bar{v}_T^2 (H^\dagger H) - 2\lambda (H^\dagger H)^2 + \text{Yukawa terms}). \quad (28)$$

Combining these with the  $\mathcal{O}(m_\sigma^{-2})$  term, we have

$$\mathcal{L} \supset \left( \frac{abg_3^2}{m_\sigma^2} + \frac{2abg_3^2\lambda v^2}{m_\sigma^4} \right) \mathcal{Q}_{\text{HG}}^{(6)} - \frac{4adg_3^2\lambda}{m_\sigma^4} \mathcal{Q}_{\text{HG}}^{(8)}. \quad (29)$$

Via the expression for  $\Sigma_\kappa$ , this leads to a  $\lambda$  dependence in the cross section,

$$\frac{\sigma_{\text{SMEFT}}^{\hat{\alpha}}(\mathcal{G}\mathcal{G} \rightarrow h)}{\sigma_{\text{SM}}^{\hat{\alpha},1/m_\sigma^2}(\mathcal{G}\mathcal{G} \rightarrow h)} \propto -1.7 \times 10^3 \frac{abl\bar{v}_T^4}{m_\sigma^4}, \quad (30)$$

when we incorporate the common one-loop QCD correction to  $\mathcal{Q}_{\text{HG}}^{(8)}$  to have a common tree-level dependence. This arrangement of derivative terms is consistent with the geoSMEFT conventions. However, unlike the examples in Refs. [20,36], this  $\lambda$  dependence does not signal intrinsic basis dependence in fitting to  $\Sigma_\kappa$  due to an inconsistent treatment of the theory at  $\mathcal{O}(1/\Lambda^4)$ . One can also rearrange the derivative terms as

$$\frac{abg_3^2}{2m_\sigma^4} [2\partial^2 G_{\mu\nu}^A G^{A,\mu\nu} (H^\dagger H)] \quad (31)$$

and the same  $\lambda$  dependence remains and results from the dot product in the momenta of the gluons generating  $p_h^2$ . Similarly, one can arrange the derivative terms through mapping Eq. (27) to the total derivative,

$$\frac{abg_3^2}{2m_\sigma^4} \partial^2 [G_{\mu\nu}^A G^{A,\mu\nu} (H^\dagger H)], \quad (32)$$

and  $2[\partial_\mu (G_{\mu\nu}^A G^{A,\mu\nu}) \partial_\mu (H^\dagger H)]$ . This latter term again generates the same  $\lambda$  dependence through the momentum dot product for the three-point function, with a basis choice that is an alternate to the conventions in the geoSMEFT, but still projects onto the physical three-point amplitude in a consistent fashion. This indicates that experimental constraints on  $\Sigma_\kappa$  do not introduce intrinsic basis dependence due to the  $\lambda$  dependence present in this matching example. We are not aware of any evidence that there is intrinsic basis dependence in this approach, but we caution that this matching example is not a comprehensive proof excluding the possibility of basis dependence being introduced.

## VII. CONCLUSIONS

In this paper we have explored the theory uncertainty on  $\sigma(\mathcal{G}\mathcal{G} \rightarrow h)$  from higher-order terms in the SMEFT framework, and how that uncertainty is affected by which pieces of the SMEFT calculation are retained when fitting experimental data. This study was made possible by the calculation of  $\sigma(\mathcal{G}\mathcal{G} \rightarrow h)$  in Ref. [18], the first analysis to include both complete  $\mathcal{O}(1/\Lambda^4)$  effects and one-loop corrections to  $\mathcal{O}(1/\Lambda^2)$  terms. We explored three ways

of splitting the full  $\mathcal{O}(1/\Lambda^4)$ ,  $\mathcal{O}(1/16\pi^2\Lambda^2)$  result into a subset used for fitting experimental data, and a remainder that defines the uncertainty: (i) fitting experimental data with the linear  $\mathcal{L}^{(6)}$  piece only [in which case the uncertainty is all of Eq. (11) except the terms linear in  $C_{\text{HG}}^{(6)}$ ], (ii) fitting with the linear and quadratic  $\mathcal{L}^{(6)}$  pieces, and (iii) fits including select  $\mathcal{L}^{(8)}$  terms. Defined in this fashion, the theory error is controlled primarily by the dimensionful scale  $\Lambda$  and can be combined in quadrature with the experimental uncertainty.

Cases (ii) and (iii) are unconventional as they contain only a subset of higher-order results; however, they capture physics that case (i) cannot, such as a relative suppression in interference terms relative to  $(\mathcal{L}^{(6)})^2$  terms originating from the fact that  $gg \rightarrow h$  is a one-loop process in the SM. Incorporating  $C_{\text{HG}}^{(8)}$  terms into the fit, forming a combination with  $C_{\text{HG}}^{(6)}$  and  $(C_{\text{HG}}^{(6)})^2$  that we defined as  $\Sigma_k$ , further stabilizes the theory uncertainty when assuming a tree/loop hierarchy of Wilson coefficients. We found that the field redefinition ambiguities in cases (ii) and (iii) are small, suppressed by interference with the SM amplitude, and the type of basis dependence  $\propto \lambda$ , the Higgs quartic, observed in Refs. [20,36] does not appear to arise.

When extracting numerical results, we explored two different Wilson coefficient sampling schemes: all coefficients the same, and alternatively a tree/loop hierarchy. While obviously not exhaustive, these two schemes span a wide class of UV scenarios; for other setups, one could repeat the steps here starting with the result in Ref. [18].

Finally, we wish to stress that the loop nature of  $\sigma(\mathcal{G}\mathcal{G} \rightarrow h)$  in the SM plays a crucial role in the validity of including partial  $\mathcal{O}(1/\Lambda^4)$  results when comparing with experiment, as it suppresses field redefinition ambiguities on the quadratic term (independent of the Wilson coefficient matching scheme). We strongly stress that our conclusions do not generally apply to the case where a tree-level SM amplitude is present to interfere with SMEFT perturbations. When retaining partial  $\mathcal{O}(1/\Lambda^4)$  terms in a projection of experimental results in such a case, numerical ambiguities can be  $\mathcal{O}(1)$ .

## ACKNOWLEDGMENTS

M. T. acknowledges the Villum Fund, Project No. 00010102. The work of A. M. was supported in part by the National Science Foundation under Grants No. PHY-1820860 and No. PHY-2112540. We thank Tyler Corbett, Chris Hays, and Andreas Helset for insightful discussions.

## APPENDIX A: THEORY ERROR NUMERICAL ESTIMATES

An alternative approach to illustrating the effect of higher-order terms leading to theory error estimates is to set  $C_{\text{HG}}^{(6)}$  to a fixed value, and then illustrate the resulting

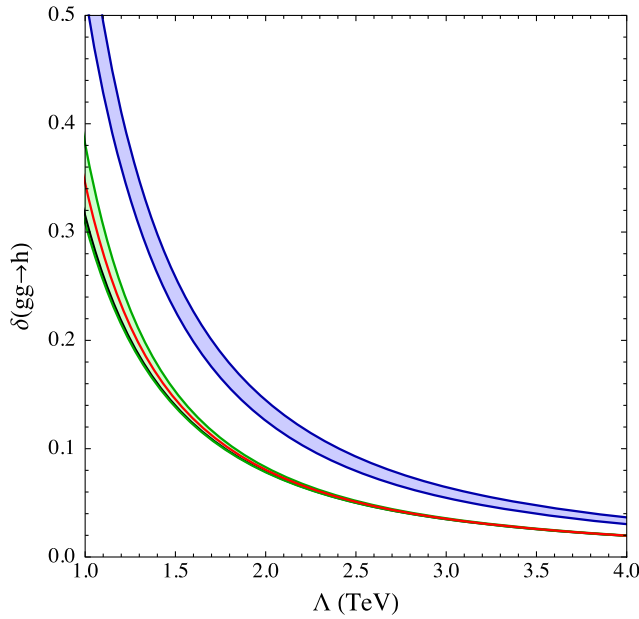


FIG. 2. Deviation in  $\sigma(\mathcal{G}\mathcal{G} \rightarrow h)$  relative to the SM with  $C_{\text{HG}}^{(6)} = 0.01$ , and all other coefficients sampled according to Gaussian distributions with zero mean and width 0.01. The deviation is plotted as a function of  $\Lambda$ . The black (red) lines correspond to the linear (quadratic)  $C_{\text{HG}}^{(6)}$  terms, the green band is the  $2\sigma$  band that results from 10 000 samples of the  $\mathcal{O}(1/\Lambda^4)$  corrections, and the blue band is the  $2\sigma$  band from 10 000 samples of the sum of the  $\mathcal{O}(1/\Lambda^4)$  and loop-level,  $\mathcal{O}(1/16\pi^2\Lambda^2)$  terms.

change in the induced deviation in  $\sigma(\mathcal{G}\mathcal{G} \rightarrow h)$  when the higher-order coefficients are varied over assumed distributions.

These results are shown in Figs. 2–4. In each of the figures, the black and red lines indicate the contribution to Eq. (11) from the linear and quadratic  $C_{\text{HG}}^{(6)}$  terms, respectively. The green band shows the range of values when the  $\mathcal{O}(1/\Lambda^4)$  terms are included, and the blue band shows the range once  $\mathcal{O}(1/\Lambda^4)$  and “loop,”  $\mathcal{O}(1/16\pi^2\Lambda^2)$  terms are included. The range of values corresponds to  $2\sigma$  values, derived from sampling the coefficients in the higher-order [ $\mathcal{O}(1/\Lambda^4)$  or  $\mathcal{O}(1/16\pi^2\Lambda^2)$ ] terms 10 000 times from Gaussian distributions and extracting the standard deviation of the collection. The differences between the figures are the assumptions made on the Wilson coefficients; in Fig. 2, we set  $C_{\text{HG}}^{(6)} = 0.01$  and sample the higher-order terms according to a Gaussian with zero mean and width 0.01, in Fig. 3 we use 1.0 for the value of  $C_{\text{HG}}^{(6)}$  and the width of the sampling Gaussians, and in Fig. 4 we use a tree/loop scheme, setting  $C_{\text{HG}}^{(6)} = 0.01$  and using 1.0/0.01 for the width of the Gaussians for operators that fall into the tree/loop category. The horizontal axes of the three figures have been chosen such that the (absolute value of the) deviation in  $\sigma(\mathcal{G}\mathcal{G} \rightarrow h)$  is less than 0.5.

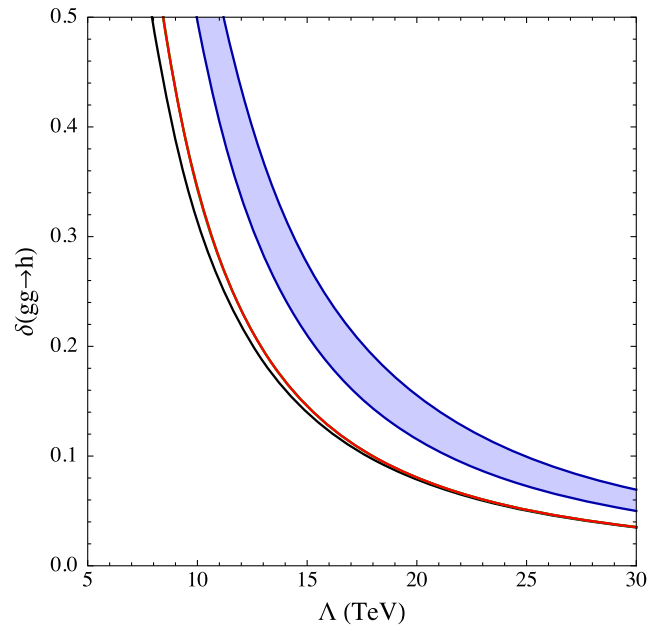


FIG. 3. Deviation in  $\sigma(\mathcal{G}\mathcal{G} \rightarrow h)$  relative to the SM with  $C_{\text{HG}}^{(6)} = 1.0$ , and all other coefficients sampled according to Gaussian distributions with zero mean and width 1.0. The deviation is plotted as a function of  $\Lambda$ . The black (red) lines correspond to the linear (quadratic)  $C_{\text{HG}}^{(6)}$  terms, the green band is the  $2\sigma$  band that results from 10 000 samples of the  $\mathcal{O}(1/\Lambda^4)$  corrections, and the blue band is the  $2\sigma$  band from 10 000 samples of the sum of the  $\mathcal{O}(1/\Lambda^4)$  and loop-level,  $\mathcal{O}(1/16\pi^2\Lambda^2)$  terms.

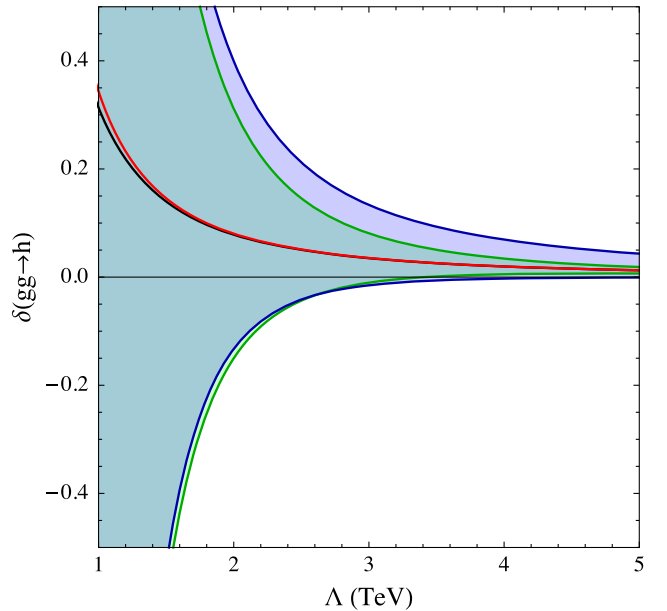


FIG. 4. Deviation in  $\sigma(\mathcal{G}\mathcal{G} \rightarrow h)$  relative to the SM with  $C_{\text{HG}}^{(6)} = 0.01$ , and all other coefficients sampled according to Gaussian distributions with zero mean and width of either 1.0 or 0.01 depending on whether the corresponding operator is generated at tree or loop level following the classification in Refs. [14–16]. The deviation is plotted as a function of  $\Lambda$ , and the color scheme for the lines and bands is the same as in Figs. 2 and 3.

## APPENDIX B: ADDITIONAL THEORY ERROR ESTIMATES

Here we apply the numerical error analysis technique from Sec. V to  $\Gamma(h \rightarrow \gamma\gamma)$ ;  $\Gamma(h \rightarrow \gamma\gamma)$  is also a loop-level process in the SM and therefore subject to similar questions as  $\sigma(\mathcal{GG} \rightarrow h)$  regarding which SMEFT contributions to keep when projecting experimental results and the impact of higher-order terms. The full SMEFT expression to  $\mathcal{O}(v_T^2/16\pi^2\Lambda^2)$ ,  $\mathcal{O}(v_T^4/\Lambda^4)$  was derived in Ref. [18]:

$$\frac{\Gamma_{\text{SMEFT}}^{\hat{m}_W}}{\Gamma_{\text{SM}}^{\hat{m}_W}} \simeq 1 - 788f_1^{\hat{m}_W} \quad (\text{B1})$$

$$\begin{aligned} &+ 394^2(f_1^{\hat{m}_W})^2 - 351(\tilde{C}_{HW}^{(6)} - \tilde{C}_{HB}^{(6)})f_3^{\hat{m}_W} + 2228\delta G_F^{(6)}f_1^{\hat{m}_W} + 979\tilde{C}_{HD}^{(6)}(\tilde{C}_{HB}^{(6)} + 0.80\tilde{C}_{HW}^{(6)} - 1.02\tilde{C}_{HWB}^{(6)}) \\ &- 788\left[\left(\tilde{C}_{H\Box}^{(6)} - \frac{\tilde{C}_{HD}^{(6)}}{4}\right)f_1^{\hat{m}_W} + f_2^{\hat{m}_W}\right] + 2283\tilde{C}_{HWB}^{(6)}(\tilde{C}_{HB}^{(6)} + 0.66\tilde{C}_{HW}^{(6)} - 0.88\tilde{C}_{HWB}^{(6)}) - 1224(f_1^{\hat{m}_W})^2 - 117\tilde{C}_{HB}^{(6)} - 23\tilde{C}_{HW}^{(6)} \\ &+ \left[51 + 2\log\left(\frac{\hat{m}_h^2}{\Lambda^2}\right)\right]\tilde{C}_{HWB}^{(6)} + \left[-0.55 + 3.6\log\left(\frac{\hat{m}_h^2}{\Lambda^2}\right)\right]\tilde{C}_W^{(6)} + \left[27 - 28\log\left(\frac{\hat{m}_h^2}{\Lambda^2}\right)\right]\text{Re}\tilde{C}_{uB}^{(6)} \\ &+ \left[14 - 15\log\left(\frac{\hat{m}_h^2}{\Lambda^2}\right)\right]\text{Re}\tilde{C}_{uW}^{(6)} + 0.56\text{Re}\tilde{C}_{uH}^{(6)} - 0.31\text{Re}\tilde{C}_{dH}^{(6)} + 2\tilde{C}_{H\Box}^{(6)} - \frac{\tilde{C}_{HD}^{(6)}}{2} + 2.0\tilde{C}_{HD}^{(6)} - 7.5\tilde{C}_{HWB}^{(6)} - 3\sqrt{2}\delta G_F^{(6)} \quad (\text{B2}) \end{aligned}$$

in the  $\hat{m}_W$  scheme, and

$$\begin{aligned} \frac{\Gamma_{\text{SMEFT}}^{\hat{\alpha}_{ew}}}{\Gamma_{\text{SM}}^{\hat{\alpha}_{ew}}} &\simeq 1 - 758f_1^{\hat{\alpha}_{ew}} + 379^2(f_1^{\hat{\alpha}_{ew}})^2 - 350(\tilde{C}_{HW}^{(6)} - \tilde{C}_{HB}^{(6)})^2 - 1159(f_1^{\hat{\alpha}_{ew}})^2 - 61\tilde{C}_{HWB}^{(6)}(\tilde{C}_{HB}^{(6)} + 7.2\tilde{C}_{HW}^{(6)} - 9.2\tilde{C}_{HWB}^{(6)}) \\ &- 13.5\tilde{C}_{HD}^{(6)}(\tilde{C}_{HB}^{(6)} + 16\tilde{C}_{HW}^{(6)} - 15\tilde{C}_{HWB}^{(6)}) + 1383\delta G_F^{(6)}(\tilde{C}_{HB}^{(6)} - 0.13\tilde{C}_{HW}^{(6)} - 0.15\tilde{C}_{HWB}^{(6)}) \\ &- 758\left[\left(\tilde{C}_{H\Box}^{(6)} - \frac{\tilde{C}_{HD}^{(6)}}{4}\right)f_1^{\hat{\alpha}_{ew}} + f_2^{\hat{\alpha}_{ew}}\right] - 218\tilde{C}_{HB}^{(6)} + 22\tilde{C}_{HW}^{(6)} + \left[-17 + 2.0\log\left(\frac{\hat{m}_h^2}{\Lambda^2}\right)\right]\tilde{C}_{HWB}^{(6)} \\ &+ \left[-0.60 + 3.6\log\left(\frac{\hat{m}_h^2}{\Lambda^2}\right)\right]\tilde{C}_W^{(6)} + \left[26 - 27\log\left(\frac{\hat{m}_h^2}{\Lambda^2}\right)\right]\text{Re}\tilde{C}_{uB}^{(6)} + \left[14 - 15\log\left(\frac{\hat{m}_h^2}{\Lambda^2}\right)\right]\text{Re}\tilde{C}_{uH}^{(6)} + 0.56\text{Re}\tilde{C}_{dH}^{(6)} \\ &- 0.31\text{Re}\tilde{C}_{dH}^{(6)} + 2\tilde{C}_{H\Box}^{(6)} - \frac{\tilde{C}_{HD}^{(6)}}{2} - \sqrt{2}\delta G_F^{(6)} \quad (\text{B3}) \end{aligned}$$

in the  $\hat{\alpha}_{ew}$  scheme. Here,  $C_{HB}^{(6+2n)}$ ,  $C_{HW}^{(6+2n)}$ ,  $C_{HW,2}^{(8)}$ ,  $C_{HWB}^{(6+2n)}$ ,  $C_{uH}^{(6)}$ ,  $C_{uB}^{(6)}$ , and  $C_W^{(6)}$  are the Wilson coefficients of the following operators:

$$\begin{aligned} \mathcal{Q}_{HB}^{(6+2n)} &= (H^\dagger H)^{(1+n)} B^{\mu\nu} B_{\mu\nu}, \\ \mathcal{Q}_{HW}^{(6+2n)} &= (H^\dagger H)^{(1+n)} W_a^{\mu\nu} W_{\mu\nu}^a, \\ \mathcal{Q}_{HW,2}^{(8)} &= (H^\dagger \sigma_a H)(H^\dagger \sigma_b H) W_a^{\mu\nu} W_{\mu\nu}^b, \\ \mathcal{Q}_{HWB}^{(6+2n)} &= (H^\dagger \sigma_a H)(H^\dagger H)^{(n)} W_{\mu\nu}^a B^{\mu\nu}, \\ \mathcal{Q}_{uH}^{(6)} &= (H^\dagger H)(\bar{q}_r u_r \tilde{H}), \\ \mathcal{Q}_{uB}^{(6)} &= (\bar{q}_r \sigma^{\mu\nu} u_r) \tilde{H} B^{\mu\nu}, \\ \mathcal{Q}_W^{(6)} &= \epsilon^{IJK} W_\mu^{L,\nu} W_\nu^{J,\rho} W_\rho^{K,\mu}. \quad (\text{B4}) \end{aligned}$$

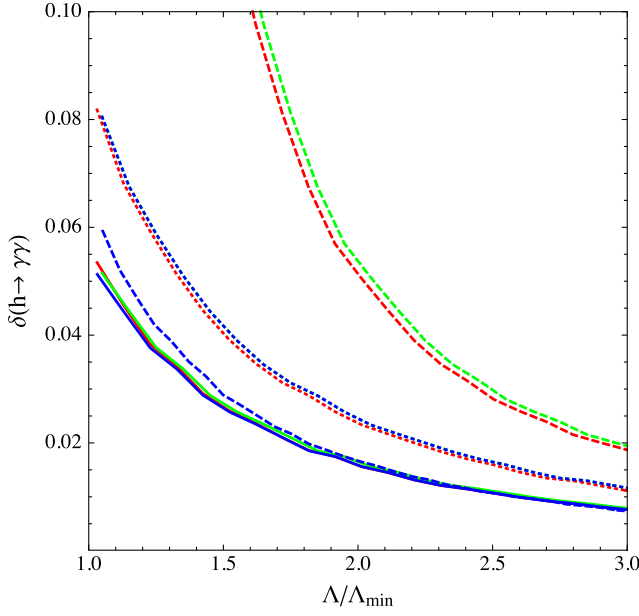


FIG. 5. Uncertainty on  $\Gamma(h \rightarrow \gamma\gamma)$  from higher-order terms in the  $\hat{m}_W$  scheme. The different colored lines correspond to different ways of breaking up the SMEFT calculation into a piece that is compared to experiment and a higher-order correction. The red lines correspond to projecting the data onto Wilson coefficients using the dimension-six interference term ( $f_1$ ) only, the green lines correspond to including the  $f_1$  and  $(f_1)^2$  pieces, and the blue line corresponds to including  $f_1$ ,  $(f_1)^2$ , and  $f_2$ . The solid lines correspond to a coefficient matching scheme where all coefficients are 0.01, the dotted lines correspond to all coefficients equal to 1, and the dashed lines correspond to the tree/loop scheme with values 1.0/0.01.

$f_i^{\hat{m}_W} \cong f_i^{\hat{\alpha}_{ew}}$  are linear combinations of Wilson coefficients:

$$f_1^{\hat{m}_W} = [\tilde{C}_{HB}^{(6)} + 0.29\tilde{C}_{HW}^{(6)} - 0.54\tilde{C}_{HWB}^{(6)}], \quad (\text{B5})$$

$$f_2^{\hat{m}_W} = [\tilde{C}_{HB}^{(8)} + 0.29(\tilde{C}_{HW}^{(8)} + \tilde{C}_{HW,2}^{(8)}) - 0.54\tilde{C}_{HWB}^{(8)}], \quad (\text{B6})$$

$$f_3^{\hat{m}_W} = [\tilde{C}_{HW}^{(6)} - \tilde{C}_{HB}^{(6)} - 0.66\tilde{C}_{HWB}^{(6)}]. \quad (\text{B7})$$

Following the analysis of  $\sigma(\mathcal{GG} \rightarrow h)$ , we break up the full result for  $\Gamma(h \rightarrow \gamma\gamma)$  into three cases:

- (i) Retain only the dimension-six interference piece,  $\propto f_1$ , when comparing with experiment. The loop corrections for  $\Gamma(h \rightarrow \gamma\gamma)$  are not  $\propto f_1$  [41], so in this case we only keep the tree-level interference term.
- (ii) Retain the interference piece plus  $(f_1)^2$  terms, the square of the dimension-six piece from (i).
- (iii) Retain the  $f_1$ ,  $(f_1)^2$ , and  $f_2$  terms.

In each case, we associate the remainder of Eqs. (B2)–(B3) with the impact from higher-order terms and explore its numerical impact using the same two Wilson coefficient matching schemes used in the main text.

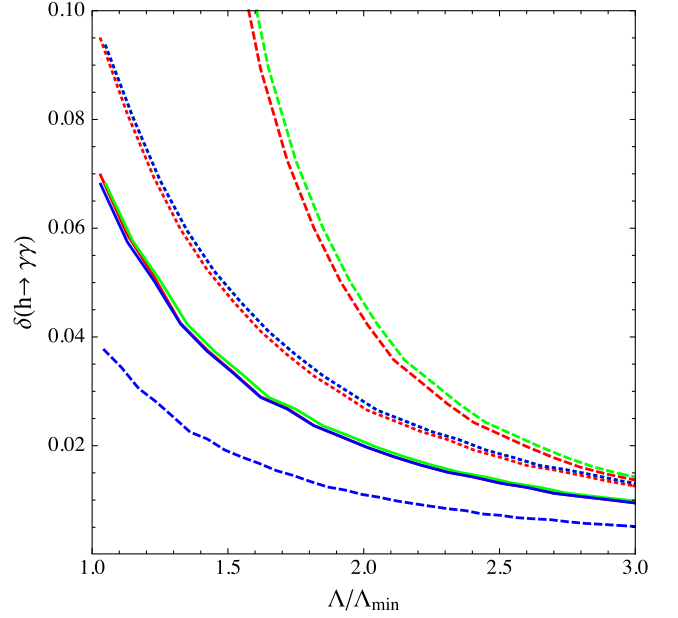


FIG. 6. Uncertainty on  $\Gamma(h \rightarrow \gamma\gamma)$  from higher-order terms in the  $\hat{\alpha}_{ew}$  scheme. The color and dashed scheme is the same as in Fig. 5.

We next determine the minimum scale  $\Lambda_{\min}$  by equating the retained part of  $\Gamma(h \rightarrow \gamma\gamma)$  to the current uncertainty on  $gg \rightarrow h \rightarrow \gamma\gamma$ ,  $\delta\mu_{gg \rightarrow h \rightarrow \gamma\gamma} = 0.14$  [37] and setting Wilson coefficients according to the matching scheme. Then, for  $\Lambda > \Lambda_{\min}$ , we evaluate the higher-order piece 10 000 times, evaluating the higher-order terms at each step using values drawn from Gaussian distributions with the width set by the matching scheme. The standard deviation from the collection of higher-order term values is shown below in Figs. 5 and 6 as a function of  $\Lambda/\Lambda_{\min}$  for the various Wilson coefficient sampling cases, matching patterns, and electroweak input schemes.<sup>8</sup>

As was the case in  $\sigma(\mathcal{GG} \rightarrow h)$ , case (iii) is the most robust under the different Wilson coefficient schemes studied here. As was the case for  $\sigma(\mathcal{GG} \rightarrow h)$ , the difference between the curves with all Wilson coefficients equal to 1 and all coefficients equal to 0.01 (when plotted vs  $\Lambda/\Lambda_{\min}$ ) can be traced to the  $\log(\Lambda^2)$  terms in  $\Gamma(h \rightarrow \gamma\gamma)$ . Additionally, comparing Figs. 5 and 6, one can see that there is some dependence on the electroweak input scheme. [We have checked that in the case of the U(1) matching model, the retention of a partial set of higher-order order terms used here does not indicate intrinsic basis dependence due to  $\lambda$  dependence.]

<sup>8</sup>Explicitly, the  $\Lambda_{\min}$  values for  $\Gamma^{\hat{m}_W}(h \rightarrow \gamma\gamma)$  are  $\Lambda_{\min} = 1.6$  TeV for all cases when the Wilson coefficients are all 0.01,  $\Lambda_{\min} = 16$  TeV for all cases when the Wilson coefficients are all 1.0, and  $\Lambda_{\min} = 1.6, 1.6, 2.5$  TeV for cases i), ii), and iii), respectively, in the tree/loop 1.0/0.01 scheme. The  $\Lambda_{\min}$  values for  $\Gamma^{\hat{\alpha}_{ew}}(h \rightarrow \gamma\gamma)$  are essentially the same.

- [1] W. Buchmuller and D. Wyler, *Nucl. Phys.* **B268**, 621 (1986).
- [2] B. Grzadkowski, M. Iskrzynski, M. Misiak, and J. Rosiek, *J. High Energy Phys.* **10** (2010) 085.
- [3] R. Alonso, E. E. Jenkins, A. V. Manohar, and M. Trott, *J. High Energy Phys.* **04** (2014) 159.
- [4] I. Brivio and M. Trott, *Phys. Rep.* **793**, 1 (2019).
- [5] I. Brivio, Y. Jiang, and M. Trott, *J. High Energy Phys.* **12** (2017) 070.
- [6] A. Helset, A. Martin, and M. Trott, *J. High Energy Phys.* **03** (2020) 163.
- [7] J. Ellis, C. W. Murphy, V. Sanz, and T. You, *J. High Energy Phys.* **06** (2018) 146.
- [8] A. Biekötter, T. Corbett, and T. Plehn, *SciPost Phys.* **6**, 064 (2019).
- [9] E. da Silva Almeida, A. Alves, N. Rosa Agostinho, O. J. P. Éboli, and M. C. Gonzalez-Garcia, *Phys. Rev. D* **99**, 033001 (2019).
- [10] S. Dawson, S. Homiller, and S. D. Lane, *Phys. Rev. D* **102**, 055012 (2020).
- [11] J. Ellis, M. Madigan, K. Mimasu, V. Sanz, and T. You, *J. High Energy Phys.* **04** (2021) 279.
- [12] J. Baglio, S. Dawson, S. Homiller, S. D. Lane, and I. M. Lewis, *Phys. Rev. D* **101**, 115004 (2020).
- [13] E. d. S. Almeida, A. Alves, O. J. P. Éboli, and M. C. Gonzalez-Garcia, *Phys. Rev. D* **105**, 013006 (2022).
- [14] C. Arzt, M. B. Einhorn, and J. Wudka, *Nucl. Phys.* **B433**, 41 (1995).
- [15] J. de Blas, J. C. Criado, M. Perez-Victoria, and J. Santiago, *J. High Energy Phys.* **03** (2018) 109.
- [16] N. Craig, M. Jiang, Y.-Y. Li, and D. Sutherland, *J. High Energy Phys.* **08** (2020) 086.
- [17] E. E. Jenkins, A. V. Manohar, and M. Trott, *J. High Energy Phys.* **09** (2013) 063.
- [18] T. Corbett, A. Martin, and M. Trott, *J. High Energy Phys.* **12** (2021) 147.
- [19] A. Helset, M. Paraskevas, and M. Trott, *Phys. Rev. Lett.* **120**, 251801 (2018).
- [20] C. Hays, A. Helset, A. Martin, and M. Trott, *J. High Energy Phys.* **11** (2020) 087.
- [21] T. Corbett, *J. High Energy Phys.* **03** (2021) 001.
- [22] B. S. DeWitt, *Phys. Rev.* **162**, 1195 (1967).
- [23] G. 't Hooft, *Nucl. Phys.* **B62**, 444 (1973).
- [24] L. F. Abbott, *Acta Phys. Pol. B* **13**, 33 (1982).
- [25] V. Cirigliano, W. Dekens, J. de Vries, and E. Mereghetti, *Phys. Rev. D* **94**, 016002 (2016).
- [26] V. Cirigliano, W. Dekens, J. de Vries, and E. Mereghetti, *Phys. Rev. D* **94**, 034031 (2016).
- [27] M. Trott, *Phys. Rev. D* **104**, 095023 (2021).
- [28] M. Dührssen, S. Heinemeyer, H. Logan, D. Rainwater, G. Weiglein, and D. Zeppenfeld, *Phys. Rev. D* **70**, 113009 (2004).
- [29] J. Espinosa, C. Grojean, M. Muhlleitner, and M. Trott, *J. High Energy Phys.* **05** (2012) 097.
- [30] D. Carmi, A. Falkowski, E. Kuflik, and T. Volansky, *J. High Energy Phys.* **07** (2012) 136.
- [31] A. Azatov, R. Contino, and J. Galloway, *J. High Energy Phys.* **04** (2012) 127; **04** (2013) 140(E).
- [32] A. David, A. Denner, M. Dührssen, M. Grazzini, C. Grojean, G. Passarino, M. Schumacher, M. Spira, G. Weiglein, and M. Zanetti (LHC Higgs Cross Section Working Group), [arXiv:1209.0040](https://arxiv.org/abs/1209.0040).
- [33] I. Brivio, T. Corbett, and M. Trott, *J. High Energy Phys.* **10** (2019) 056.
- [34] G. Buchalla, O. Cata, A. Celis, and C. Krause, *Phys. Lett. B* **750**, 298 (2015).
- [35] G. Buchalla, O. Cata, A. Celis, and C. Krause, *Eur. Phys. J. C* **76**, 233 (2016).
- [36] T. Corbett, A. Helset, A. Martin, and M. Trott, *J. High Energy Phys.* **06** (2021) 076.
- [37] G. Aad, B. Abbott, D. C. Abbott, O. Abdinov, A. Abed Abud, K. Abeling, D. K. Abhayasinghe, S. H. Abidi, O. S. AbouZeid, N. L. Abraham *et al.* (ATLAS Collaboration), *Phys. Rev. D* **101**, 012002 (2020).
- [38] The CMS Collaboration, Combined Higgs boson production and decay measurements with up to  $137 \text{ fb}^{-1}$  of proton-proton collision data at  $\sqrt{s} = 13 \text{ TeV}$ , Technical Report No. CMS-PAS-HIG-19-005, CERN, Geneva, 2020.
- [39] C. Degrande, J. M. Gerard, C. Grojean, F. Maltoni, and G. Servant, *J. High Energy Phys.* **07** (2012) 036; **03** (2013) 032(E).
- [40] B. Henning, X. Lu, and H. Murayama, *J. High Energy Phys.* **01** (2016) 023.
- [41] C. Hartmann and M. Trott, *J. High Energy Phys.* **07** (2015) 151.